激光表面处理对工业级锆基块体非晶合金塑性变形能力的影响

程杨洋[1]，钟勇[2]，张星[1]，陈辰[3]，余龙[4]，王鹏飞[1]，张涛[5*]

（1.中国航天科技创新研究院，北京 100176；2.西南技术工程研究所，重庆 400039；3.郑州大学，郑州 450001；4.中南大学，长沙 410083；5.北京航空航天大学，北京 100191）

摘要：目的 针对工业级 $Zr_{49.7}Ti_2Cu_{37.8}Al_{10}Er_{0.5}$ 块体非晶合金受到原材料中杂质元素和制备环境中氧元素的影响，其本征塑性变形能力较差的问题，研究激光表面处理对工业级 $Zr_{49.7}Ti_2Cu_{37.8}Al_{10}Er_{0.5}$ 块体非晶合金在压缩和拉伸条件下塑性变形能力的影响。**方法** 采用低纯原料制备工业级母合金锭子，利用铜模铸造法在低真空环境下制备工业级非晶合金试样，采用激光法对试样进行表面处理，利用万能试验机对激光处理试样的压缩和拉伸力学性能进行测试。通过 X 射线衍射仪和电子探针对试样的微观组织结构进行表征，采用扫描电镜对力学测试失效后试样的形貌进行微尺度观察。**结果** 经激光表面处理后影响区的深度约为 150 μm，在影响区内铜元素的含量有所降低，但依然为非晶结构。在压缩条件下，未经激光表面处理的工业级 $Zr_{49.7}Ti_2Cu_{37.8}Al_{10}Er_{0.5}$ 块体非晶合金的塑性应变为 0，断裂强度为 1 534 MPa。经过激光表面处理后，试样具有 1%的塑性应变，屈服强度为 1 337 MPa，断裂强度为 1 562 MPa。在拉伸条件下，激光表面处理前后工业级块体非晶合金的塑性应变均为 0，断裂强度也无明显变化，其平均值为 1 379 MPa。**结论** 通过激光表面处理在工业级 $Zr_{49.7}Ti_2Cu_{37.8}Al_{10}Er_{0.5}$ 块体非晶合金试样表面引起的成分变化和引入的残余应力状态，能够有效促使压缩载荷作用下剪切带的萌生，提高其压缩塑性变形能力。

关键词：工业级块体非晶合金；激光表面处理；塑性变形；断裂强度；剪切带

中图分类号：TG139 **文献标志码：**A **文章编号：**1001-3660(2024)05-0166-08

DOI：10.16490/j.cnki.issn.1001-3660.2024.05.017

Effect of Laser Surface Treatment on Plastic Deformation of Industrial-grade Zr-based Bulk Metallic Glasses

CHENG Yangyang[1], ZHONG Yong[2], ZHANG Xing[1], CHEN Chen[3], YU Long[4], WANG Pengfei[1], ZHANG Tao[5]*

(1. China Academy of Aerospace Science and Innovation, Beijing 100176, China; 2. Southwest Institute of Technology and Engineering, Chongqing 400039, China; 3. Zhengzhou University, Zhengzhou 450001, China; 4. Central South University, Changsha 410083, China; 5. Beihang University, Beijing 100191, China)

ABSTRACT: Industrial-grade $Zr_{49.7}Ti_2Cu_{37.8}Al_{10}Er_{0.5}$ bulk metallic glasses (BMGs) possess poor plastic deformation ability due

收稿日期：2022-11-26；**修订日期：**2023-05-10

Received：2022-11-26；**Revised：**2023-05-10

基金项目：国家自然科学基金（12202006，52274399）

Fund：National Natural Science Foundation of China (12202006, 52274399)

引文格式：程杨洋，钟勇，张星，等. 激光表面处理对工业级锆基块体非晶合金塑性变形能力的影响[J]. 表面技术, 2024, 53(5): 166-173.

CHENG Yangyang, ZHONG Yong, ZHANG Xing, et al. Effect of Laser Surface Treatment on Plastic Deformation of Industrial-grade Zr-based Bulk Metallic Glasses[J]. Surface Technology, 2024, 53(5): 166-173.

*通信作者（Corresponding author）

to the effect of impurity elements in the raw materials and oxygen elements from the preparation processing. This paper aims to study the effect of the laser surface treatment (LSM) on the microstructure and the plasticity of industrial-grade $Zr_{49.7}Ti_2Cu_{37.8}Al_{10}Er_{0.5}$ BMGs. The master alloy ingots were prepared by arc-melting with low-purity raw materials. The industrial-grade $Zr_{49.7}Ti_2Cu_{37.8}Al_{10}Er_{0.5}$ BMG specimens were prepared by copper mold casting method in a low vacuum environment, and then the specimens were treated by LSM under different parameters. The compressive and tensile properties of the laser treated specimens were investigated with a universal testing machine. The microstructure of the specimens before and after the LSM was characterized with an X-ray diffractometer and an electron microprobe. The morphology of the specimens after the deformation was observed with a scanning electron microscopy (SEM). It was found that the depth of the affected zone induced by the LSM was about 150 μm. The content of copper element dropped in the affected zone compared with the nominal composition. Notably, the laser-affected zone in the near surface and the unaffected zone in the middle of the specimen still exhibited amorphous structure. Before the LSM, the compressive plasticity of the industrial grade $Zr_{49.7}Ti_2Cu_{37.8}Al_{10}Er_{0.5}$ BMG was nearly zero, and the fracture strength was 1 534 MPa. After the LSM, the compressive plastic strain was 1% with the yielding strength 1 478 MPa and the fracture strength 1 562 MPa. The SEM observation demonstrated that there existed numerous shear bands on the laser-treated specimens while it was hard to detect shear bands on the specimens without LSM. The appearance of the shear bands further proved the plastic deformation on the laser-treated specimens. Additionally, the fracture surfaces of all the specimens possessed vein-like patterns typical of BMGs, and the angle between the fracture surface and the loading direction was less than 45°, indicating that the shear failure mode was not affected by the LSM. On the other hand, under the tensile condition, the plastic strain of the specimens before and after the LSM was zero, and there was no obvious change in the fracture strength (1 390 MPa). It was known that the LSM produced the residual stress and the change of amorphous composition. During the loading, the combination of the residual stress and the external stress induced the stress concentration and stress gradient which facilitated the formation of the shear band and prevented its propagation. The difference in amorphous composition lead to the different characteristics of shear bands and intensified the interaction of shear bands. Based on the experimental results, it is confirmed that the LSM can effectively improve the compressive plasticity of the industrial-grade $Zr_{49.7}Ti_2Cu_{37.8}Al_{10}Er_{0.5}$ BMG. Nevertheless, the existence of oxygen and erbium elements are detrimental to the inherent plastic deformability of the industrial-grade $Zr_{49.7}Ti_2Cu_{37.8}Al_{10}Er_{0.5}$ BMG. Accordingly, the compositional change and the residual stress at the present scale cannot counteract the effect of the tensile normal stress on the crack initiation.

KEY WORDS: industrial-grade bulk metallic glass; laser surface treatment; plastic deformation; fracture strength; shear bands

块体非晶合金独特的原子结构赋予了其不同于传统晶态合金的力学性能[1-5]。在传统晶体材料中，塑性变形通常由位错运动控制，而块体非晶合金的塑性变形由剪切带控制[1-2,4]。由于促使位错运动的应力小于促使剪切带运动的应力，所以非晶合金的强度是相应晶态材料强度的 2~4 倍[6-10]。块体非晶合金在高于临界载荷的作用下，其内部结构会发生变化，产生局域应变软化，形成了高度局域化的剪切带[4,11-14]。在块体非晶合金中不存在能够有效阻碍剪切带扩展的结构，剪切带萌生后快速扩展，并失稳转变为裂纹[4,15]，所以块体非晶合金表现出极大的室温脆性[12,16]。国内外学者通过优化成分[17-18]、引入第二相[19-22]、设计人工微结构[23-26]、表面处理[27-33]等方式促进剪切带的萌生，实现其塑性变形能力的提升。

考虑到块体非晶合金作为工程结构材料应用的经济性，采用杂质含量较高的低纯原料和含氧量较高的低真空条件将是制备块体非晶合金的重要方式之一[34-36]。已有大量实验研究发现，微量的氧、氮、硅等杂质元素会显著降低块体非晶合金的玻璃形成能力和塑性变形能力[37-41]，因此有必要探究抑制和改善杂质元素弱化工业级块体非晶合金塑性变形能力的工程技术。

激光表面处理能够对材料表面进行快速加热和冷却，导致其表面结构和应力状态发生变化。研究发现，通过优化处理工艺可以实现对材料力学性能的改善[27-33,42]。同时，激光表面处理不会对材料造成结构损伤，未在材料中引入缺陷。激光表面处理能够有效实现块体非晶合金中多重剪切带的形成，进而有效地阻碍剪切带的扩展，提高其塑性变形能力[27,31,33,43-44]。这为改善工业级块体非晶合金的塑性变形能力提供了途径。

综上所述，在制备过程中引入的杂质元素和氧元素势必劣化工业级块体非晶合金的塑性变形能力，进而影响工业级块体非晶合金的潜在应用。文中将使用海绵锆和海绵钛作为原材料，选择在低真空条件下制备具有 10 mm 非晶形成能力的工业级 $Zr_{49.7}Ti_2Cu_{37.8}Al_{10}Er_{0.5}$ 块体非晶合金，将其作为模型材料，系统研究激光表面处理对其力学性能的影响，

以期提高其塑性，促进该类合金在航空航天、生物医用、电子通信等领域的潜在应用。

1　实验

该工业级块体非晶合金的名义成分为 $Zr_{49.7}Ti_2Cu_{37.8}Al_{10}Er_{0.5}$（原子数分数），使用海绵锆和海绵钛作为原材料，其杂质含量如表 1 所示。依照成分配比，称取金属原料，将其放入日本日新技研 NEW-M04C 型真空电弧熔炼炉中，利用旋片式真空泵和分子泵达到 10 mPa 的真空条件，之后通入 0.05 MPa 低纯氩气（质量分数 99.9%），反复熔炼 4 次，将合金随炉冷却后，获得母合金。这里通过铜模喷铸法制备非晶合金试样（如图 1a 所示），将熔炼均匀的母合金破碎后，置于底部开口的石英坩埚内，在 10 Pa 的工业级低真空条件下，通入 0.05 MPa 的低纯氩气，使用高频感应加热，将石英坩埚内的母合金熔化，达到适当温度后将熔体喷铸到铜模型腔内，获得特定尺寸的工业级 $Zr_{49.7}Ti_2Cu_{37.8}Al_{10}Er_{0.5}$ 块体非晶合金。

采用脉冲 Nd:YAG 激光器对试样进行激光表面处理，将制备的工业级 $Zr_{49.7}Ti_2Cu_{37.8}Al_{10}Er_{0.5}$ 块体非晶合金置于自制工作腔内，工作腔顶部为对波长 1 064 nm 激光具有良好透射性的石英玻璃，在工作腔内部充入低纯氩气，如图 1b 所示。通过激光工作台移动控制软件，对激光的搭接率、扫描速度、方向、区域进行调控。在激光表面处理过程中，固定激光脉冲宽度为 1 ms，光斑直径为 0.8 mm，激光频率为 8 Hz。通过改变激光功率密度和扫描速度对块体非晶合金试样进行处理，选择 3 组参数：能量密度为 0.55 J/m^2，扫描速度为 100 mm/min；能量密度为 0.55 J/m^2，扫描速度为 150 mm/min；能量密度为 0.44 J/m^2，扫描速度为 250 mm/min。

表 1　海绵锆和海绵钛的成分
Tab.1 Composition of sponge Zr and sponge Ti

Elements	Mass fraction/%									
	Zr+Hf	Ti	O	Mg	Cr	Mn	Si	C	Cl	Bal.
Sponge Zr	⩾99.4	0.005	0.10	0.06	0.02	0.01	0.01	0.05	0.13	⩽0.215
Sponge Ti		99.6	0.08	0.07		0.01	0.03	0.03	0.08	⩽0.1

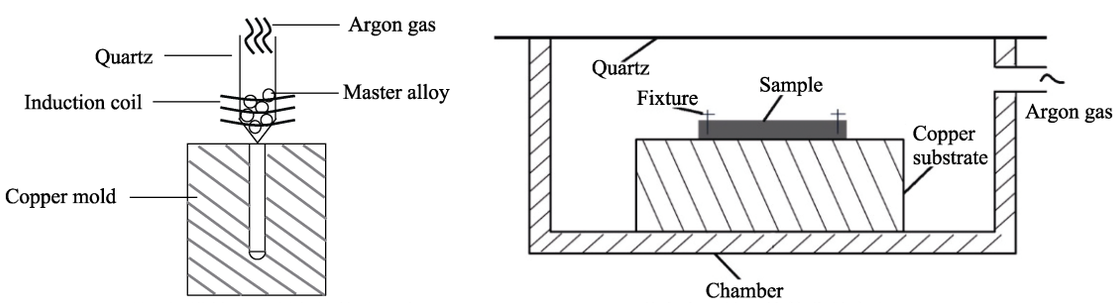

a 利用铜模铸造法制备块体非晶合金　　b 激光表面处理块体非晶合金

图 1　工业级块体非晶合金制备和激光表面处理示意图
Fig.1 Schematic diagram for manufacture of laser-treated industrial-grade BMGs: a) BMGs prepared by copper mold casting; b) BMGs treated by laser

借助 Bruker AXS D8 型 X 射线衍射仪和 JEOL JXA 8100 电子探针（EDS）及其背散射电子成像（BSE）对激光表面熔化处理前后的试样结构进行表征，通过扫描电镜（SEM）对试样的表面形貌进行观察。利用 SANS 5504 电子万能试验机对试样进行静态力学性能测试，不同实验参数试样的测试数量为 3。在压缩实验中，压缩试样尺寸为 2 mm×2 mm×4 mm，压缩应变速率为 4×10^{-4} s^{-1}，试样长径比为 2∶1。在拉伸实验中，拉伸试样尺寸如图 2 所示。通过引伸计测量试样的变形量，应变速率为 8×10^{-4} s^{-1}。

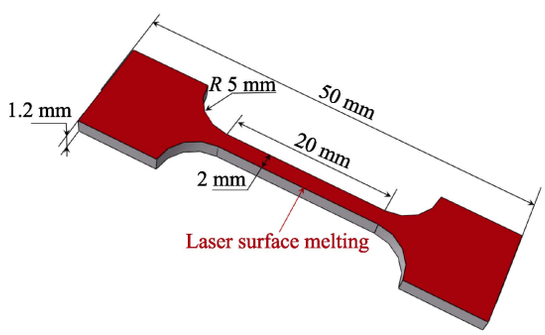

图 2　工业级 $Zr_{49.7}Ti_2Cu_{37.8}Al_{10}Er_{0.5}$ 块体非晶合金的拉伸试样尺寸
Fig.2 Dimensions of tension specimen of industrial-grade $Zr_{49.7}Ti_2Cu_{37.8}Al_{10}Er_{0.5}$ BMGs

2　结果与分析

2.1　微观组织结构分析

铸态试样和激光处理试样表面及其芯部截面的 XRD 图谱如图 3 所示。所有试样的 X 射线衍射花样表现为“馒头”状的漫散射峰，由此可以判断试样在经过激光处理后依然为全非晶结构。值得注意的是，Cheng 等[28]研究发现，经激光表面处理后 Cu-Zr-Al 块体非晶合金体系的试样表层的 Cu 元素含量明显减少，导致“馒头”峰发生明显偏移；文中试样表面 XRD 衍射峰与铸态试样及试样芯部激光未影响区相比，其馒头峰未发生明显偏移，最高峰在 44°处，表明激光表面处理并未显著改变该试样表层的成分和结构。

经激光处理后，试样的 BSE 图如图 4 所示，试样表层和芯部的 EDS 分析结果如表 2 所示。从图 4a~c 中可以发现，在激光扫描速度 100、150 mm/min 下处理后，表层和芯部的成分存在明显的衬度差异，表明 2 个区域的成分发生了变化；表层成分变化区的厚度约为 100 μm，整个试样形成了一种三明治结构；在激光扫描速度 250 mm/min 下处理后，试样表层和芯部未出现明显的成分衬度差异。进一步利用 EDS 对激光表面处理前后试样的成分进行半定量表征，结果如表 2 所示。所有试样的铝元素含量比名义成分中的铝元素含量低，这种差异可能是由电弧熔炼过程中铝元素的挥发所致。在激光扫描速度 100、150 mm/min

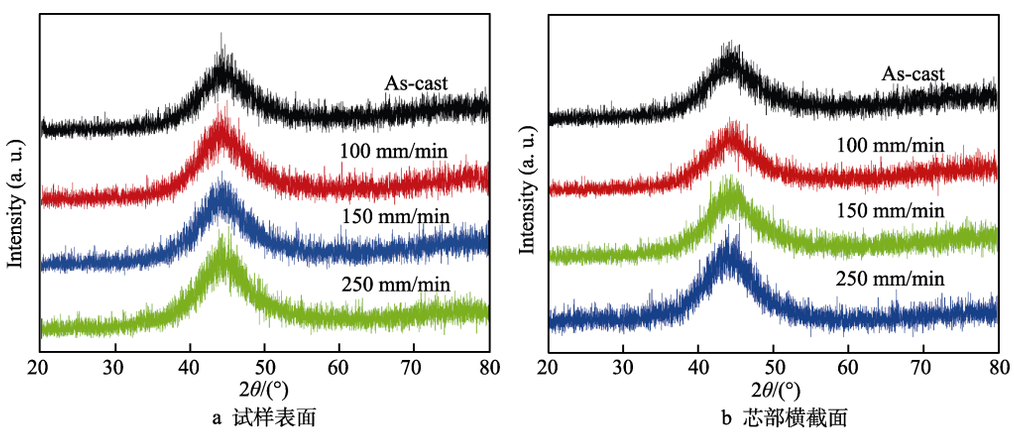

图 3　工业级 $Zr_{49.7}Ti_2Cu_{37.8}Al_{10}Er_{0.5}$ 块体非晶合金铸态试样及经不同激光工艺参数处理后试样的 XRD 图谱

Fig.3 XRD patterns of industrial-grade $Zr_{49.7}Ti_2Cu_{37.8}Al_{10}Er_{0.5}$ BMGs before and after laser treatment under different parameters: a) surface of specimen; b) cross-section of core

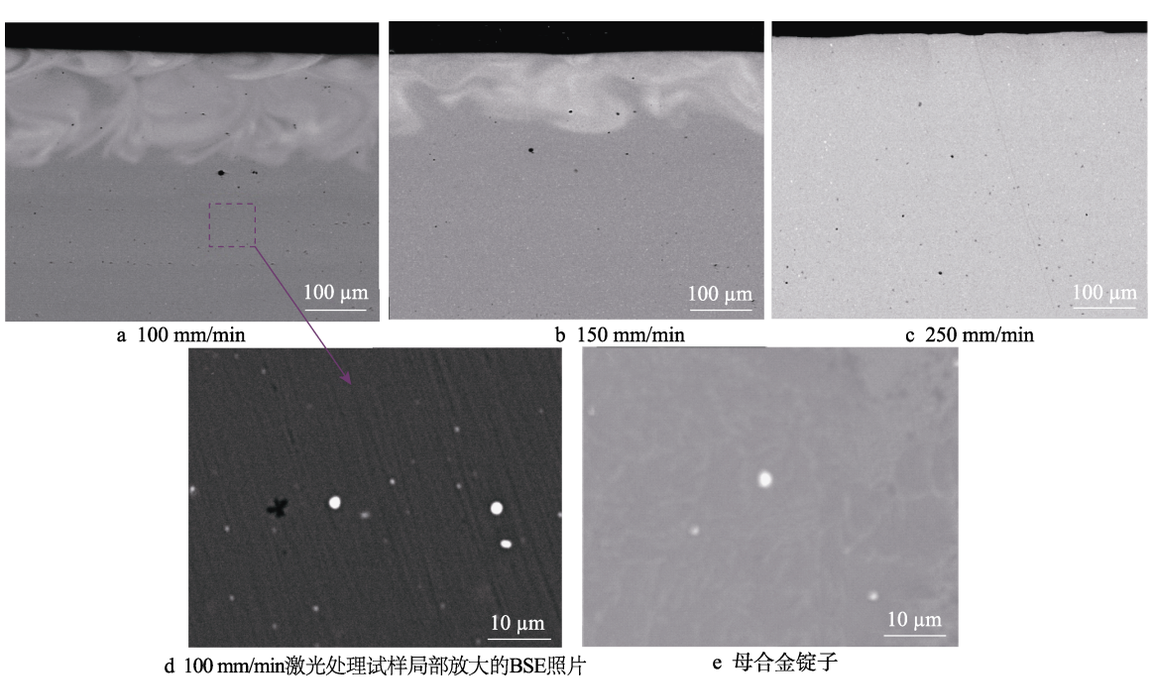

图 4　工业级 $Zr_{49.7}Ti_2Cu_{37.8}Al_{10}Er_{0.5}$ 块体非晶合金经不同激光工艺参数处理后试样及母合金锭子的 BSE 照片

Fig.4 BSE images of industrial-grade $Zr_{49.7}Ti_2Cu_{37.8}Al_{10}Er_{0.5}$ BMGs after LSM and master ingots: a) 100 mm/min; b) 150 mm/min; c) 250 mm/min; d) enlarged image of 100 mm/min; e) master alloy

表 2　工业级 $Zr_{49.7}Ti_2Cu_{37.8}Al_{10}Er_{0.5}$ 块体非晶合金铸态试样名义成分和激光处理试样的 EDS 分析结果及影响区深度

Tab.2 Nominal composition of industrial-grade $Zr_{49.7}Ti_2Cu_{37.8}Al_{10}Er_{0.5}$ BMGs and EDS analysis & depth of affected zone of laser-treated specimens

Scanning speed	Zone	Composition	Depth/μm
As-cast		$Zr_{49.7}Ti_{2.0}Cu_{37.8}Al_{10}Er_{0.5}$	
100 mm/min	Near-surface	$Zr_{56.1}Ti_{2.1}Cu_{33.4}Al_{8.0}Er_{0.46}$	179
	Middle	$Zr_{51}Ti_{1.9}Cu_{38.4}Al_{8.2}Er_{0.47}$	
150 mm/min	Near-surface	$Zr_{53.5}Ti_{2.1}Cu_{35.8}Al_{8.1}Er_{0.5}$	
	Middle	$Zr_{51.1}Ti_{2.0}Cu_{38.0}Al_{8.4}Er_{0.5}$	129
250 mm/min	Near-surface	$Zr_{50.9}Ti_{2.0}Cu_{38.4}Al_{8.2}Er_{0.5}$	
	Middle	$Zr_{50.6}Ti_{2.0}Cu_{38.6}Al_{8.4}Er_{0.5}$	

下处理后，试样的表层与芯部相比，表层的铜元素含量偏低，表明在该区域中发生了铜元素挥发现象。试样表层和芯部区域的铜元素原子数分数的差异小于 5%。因为该工业级 $Zr_{49.7}Ti_2Cu_{37.8}Al_{10}Er_{0.5}$ 块体非晶合金在激光处理过程中铜元素挥发得较少，所以与芯部相比，表层非晶相微观结构变化较小，这与 XRD 图谱中“馒头”峰未出现明显偏移的结果一致。另外，在激光扫描速度 250 mm/min 下处理后，试样表层与芯部的成分基本相同，表明较快的激光扫描速度导致试样中激光影响区的温度升高有限，试样中的铜元素不易挥发。

此外，仔细观察 BSE 照片发现，所有试样的芯部都存在直径为 2 μm 左右的白色颗粒。如图 4d 所示，在激光扫描速度 100 mm/min 下处理后，在试样芯部的放大图像中发现数颗白色颗粒，EDS 结果显示该颗粒中氧元素和铒元素的原子数分数均在 20%以上。母合金锭子的 BSE 照片如图 4e 所示，可以看到，在母合金中也含有类似的白色颗粒，氧元素和铒元素的原子数分数都在 20%以上。由此推断，在制备母合金过程中，由于工业原料中含有氧元素，添加的微量铒元素与之发生了化学反应，从而生成了铒元素的氧化物。这也是在该工业级块体非晶合金中添加微量铒元素的目的，利用铒与氧的亲和性，达到吸氧除氧的效果，降低氧对非晶合金玻璃形成能力的影响，从而通过工业级原料和低真空度制备条件得到大尺寸块体非晶合金。利用稀土净化合金成分在铝基、镁基、铁基非晶合金中也得到了应用，其玻璃形成能力得到显著提升[45-48]。

2.2　拉伸和压缩力学性能

铸态试样和经激光处理试样的压缩−应力应变曲线如图 5a 所示。汇总了试样的屈服强度、断裂强度和塑性应变，见表 3。可以看到，铸态试样发生了显著的脆性断裂，其压缩塑性应变几乎为 0。经过激光处理后，试样的塑性得到明显提高。其中，100 mm/min 处理试样的塑性提高得最明显，为 1%。铸态试样的屈服强度平均值为 1 457 MPa，激光试样的屈服强度降低，所有试样的屈服强度平均值为 1 371 MPa。这主要是因经激光表面处理后会在试样中引入残余压应力，在压缩条件下残余压应力和外载应力正向耦合能够促使剪切带的萌生，导致试样的屈服强度降低[27,31]。不过，激光处理对试样压缩断裂强度的影响不大，所有试样的断裂强度均在 1 500 MPa 左右。

进一步借助 SEM 对压缩断裂后的试样形貌进行了观察，如图 6 所示。经激光处理后试样表面存在激光熔化形成的条纹。外载方向为纸面内垂直方向，断裂面与外载方向的夹角均小于 45°，表明试样的断裂模式为剪切变形失效[49]。如图 6a 所示，一部分铸态试样的断裂角小于 45°，一部分明显大于 45°。这可能是由试样在剪切变形裂纹形成后的扩展过程中应力状态发生变化所致，即，试样起初发生了剪切断裂，断裂角小于 45°，之后因试样发生倾斜等原因，导致其应力状态改变，产生的裂纹角度大于 45°[50]。值得注意的是，铸态试样的表面未形成明显的剪切带（图 6a），这与其为 0 的塑性应变及其较差的塑性变形能力对应。然而，塑性应变为 1%的 100 mm/min 激光

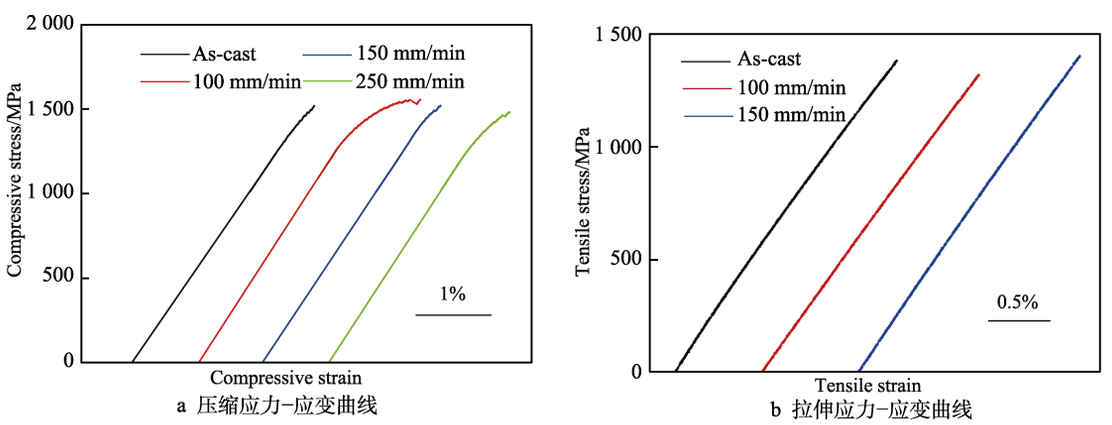

图 5　工业级 $Zr_{49.7}Ti_2Cu_{37.8}Al_{10}Er_{0.5}$ 块体非晶合金铸态试样和激光表面处理试样的应力−应变曲线

Fig.5 Representative stress-strain curves of as-cast and laser-treated industrial-grade $Zr_{49.7}Ti_2Cu_{37.8}Al_{10}Er_{0.5}$ BMGs: a) compressive stress-strain curves; b) tensile stress-train curves

表 3　工业级 $Zr_{49.7}Ti_2Cu_{37.8}Al_{10}Er_{0.5}$ 块体非晶合金激光处理前后的压缩和拉伸力学性能

Tab.3 Compressive and tensile mechanical properties of industrial-grade $Zr_{49.7}Ti_2Cu_{37.8}Al_{10}Er_{0.5}$ BMGs

Scanning speed	Compression			Tension		
	σ_y^c/MPa	σ_f^c/MPa	ε_p^c/%	σ_y^t/MPa	σ_f^t/MPa	ε_p^t/%
As-cast	1 457	1 534	0.2		1 394	0
100 mm/min	1 337	1 562	1		1 332	0
150 mm/min	1 460	1 527	0.2		1 411	0
250 mm/min	1 317	1 487	0.5			0

Note:σ and ε indicate the strength and strain, respectively. The superscript c and t indicate the compression and tension, respectively. The subscript y, f and p indicate the yielding strength, fracture strength and plastic deformation, respectively.

处理试样，其表面生成了丰富的多重剪切带（图 6b）；在经 150、250 mm/min 激光处理后仅能在试样中观察到少许剪切带（图 6c、d），这进一步证实激光表面处理能够有效改善工业级块体非晶合金的压缩塑性变形能力。

已有大量研究证实，激光表面处理在非晶合金中形成的残余应力能够促使剪切带的萌生。比如，学者们研究发现，采用激光表面处理在$(Zr_{55}Al_{10}Ni_5Cu_{30})_{99}Y_1$非晶合金表层引入残余压应力、在芯部引入残余拉应力能够改善其弯曲和压缩力学性能[31, 33-44]。Cheng 等[27-28]利用有限元模拟证实激光表面处理在试样表层引入了复杂的残余应力，存在亚毫米尺度的应力集中和应力梯度区域。同样地，文中选用工业级块体非晶合金，通过激光表面处理在试样中引入残余应力，并与外载应力耦合作用，能够在试样中形成局域的应力集中和应力梯度，有效地促进了剪切带的萌生，阻止了剪切带向裂纹的转变。

另一方面已有研究证实，纳米尺度的双相非晶合金具有优异的塑性变形能力[51-52]。双相非晶合金在成分、弹性常数上的差异能够提高剪切带在双相间扩展的能量耗散，进而抑制剪切带向裂纹的转变。由此可以推断，工业级块体非晶合金经激光处理后形成的三明治结构增加了剪切带扩展的能量耗散。同时，文中的三明治结构拥有亚毫米尺度的双相非晶，在双相中形成的剪切带存在交互作用，进一步增加了剪切带运动过程中的能量耗散。综上可知，采用激光表面处理在工业级块体非晶合金中引入残余应力和成分变化是其塑性变形得到改善的关键因素。

铸态试样和激光处理试样的拉伸应力−应变曲线如图 5b 所示。经过激光处理后，试样并未表现出一定的拉伸塑性，经过弹性变形后发生了脆性断裂，表明该三明治结构不能改善工业级块体非晶合金的拉伸力学性能。这与 Cheng 等[28]、Jiao 等[33]、Deng 等[44]在锆基块体非晶合金体系中发现激光表面处理能够优化其拉伸塑性的结果不同。对于铸态试样，其拉伸断裂强度约为 1 394 MPa，比压缩断裂强度低 140 MPa，表明存在明显的拉−压强度不对称性[53]。

造成激光表面处理未能优化工业级 $Zr_{49.7}Ti_2Cu_{37.8}Al_{10}Er_{0.5}$ 块体非晶合金拉伸塑性的主要原因有 2 个方面。一是该试样的本征塑性变形能力较差，剪切带极易演化为裂纹，导致试样在宏观塑性变形前就发生断裂[19, 54-55]。制备该试样选用的低纯原料，它含有 C、Si、Cr、Mn 等杂质元素，且加入了 Er 元素，这些元素的泊松比很低，同时泊松比较高的铜元素含量降低。已有研究指出，低泊松比元素的添加或者高泊松比元素含量的降低会劣化非晶合金的本征塑性变形能力[19, 46]。另一方面，铸造该试样时真空度较低，在铸造过程中会引入大量氧，尽管 Er 有吸收 O 元素的作用，但依然不能避免部分 O 固溶在合金中。已有研究证实，微量的氧元素会极大地削弱非晶合金的塑性变形能力[56-58]。此外，制备的试样

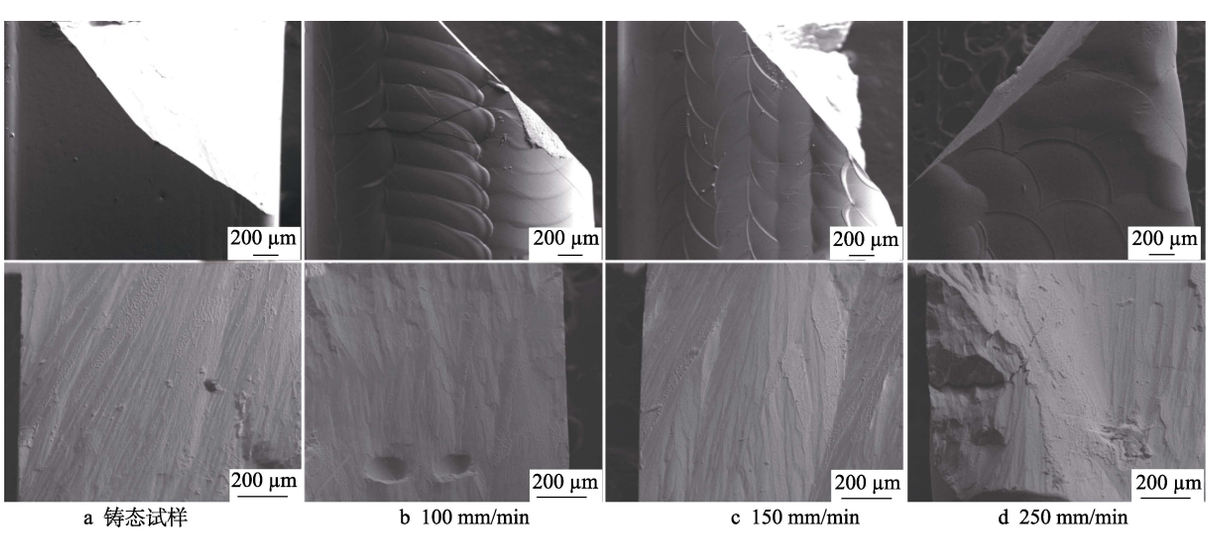

图 6　激光处理前后试样压缩断裂的侧面形貌和断面形貌

Fig.6 Side and section morphologies of compressive cracking before and after laser treatment: a) as-cast specimen; b) 100 mm/min; c) 150 mm/min; d) 250 mm/min

中存在微米级孔洞，如图 4a~c 所示，这些孔洞会成为应力集中点，致使裂纹提前出现[59]；激光表面处理未在该成分中形成能有效阻止剪切带扩展演化为裂纹的成分梯度。Cheng 等[27-28]的研究结果表明，非晶合金表面处理引起的组织结构非均质性和残余应力是提高其塑性变形能力的重要因素。通过对激光处理试样表层微观结构的分析（图 4、表 2）可以确定，该试样表层与芯部的成分衬度小于 Zhang 等[24]的研究结果，导致表层和芯部非晶结构的非均质程度较小、剪切带扩展的能量耗散减少。

3 结论

采用低纯原材料在低真空度环境下制备的工业级 $Zr_{49.7}Ti_2Cu_{37.8}Al_{10}Er_{0.5}$ 块体非晶合金的本征塑性变形能力较差，在压缩和拉伸条件下其塑性应变均接近 0。经激光表面处理后，工业级 $Zr_{49.7}Ti_2Cu_{37.8}Al_{10}Er_{0.5}$ 块体非晶合金的压缩塑性应变提高到 1%，拉伸塑性应变无明显改善。通过微观组织结构分析发现，压缩塑性的提高源于激光处理试样表面与芯部的成分差异和残余应力。在加载条件下，不同非晶结构的剪切带、不同区域的应力梯度能够有效促进剪切带的萌生，抑制剪切带的扩展，进而提高工业级块体非晶合金的压缩塑性变形能力。该方法对其拉伸塑性无显著改善效果，表明激光表面处理方法引入的成分梯度和应力梯度不能抑制拉伸正应力作用下非晶合金剪切带的软化和扩展。

参考文献：

[1] 汪卫华. 非晶态物质的本质和特性[J]. 物理学进展, 2013, 33(5): 177-351.
WANG W H. The Nature and Properties of Amorphous Matter[J]. Progress in Physics, 2013, 33(5): 177-351.

[2] 惠希东, 陈国良. 块体非晶合金[M]. 北京: 化学工业出版社, 2007: 8-10.
HUI X D, CHEN G L. Bulk Amorphous Alloy[M]. Beijing: Chemical Industry Press, 2007: 8-10.

[3] PAN J, IVANOV Y P, ZHOU W H, et al. Strain-Hardening and Suppression of Shear-Banding in Rejuvenated Bulk Metallic Glass[J]. Nature, 2020, 578: 559-562.

[4] GREER A L, CHENG Y Q, MA E. Shear Bands in Metallic Glasses[J]. Materials Science and Engineering: R: Reports, 2013, 74(4): 71-132.

[5] SCHUH C A, HUFNAGEL T C, RAMAMURTY U. Mechanical Behavior of Amorphous Alloys[J]. Acta Materialia, 2007, 55(12): 4067-4109.

[6] LI R, PANG S J, MA C L, et al. Influence of Similar Atom Substitution on Glass Formation in (La–Ce)–Al–Co Bulk Metallic Glasses[J]. Acta Materialia, 2007, 55(11): 3719-3726.

[7] PAMPILLO C A, CHEN H S. Comprehensive Plastic Deformation of a Bulk Metallic Glass[J]. Materials Science and Engineering, 1974, 13(2): 181-188.

[8] WANG J F, LI R, HUA N B, et al. Co-Based Ternary Bulk Metallic Glasses with Ultrahigh Strength and Plasticity[J]. Journal of Materials Research, 2011, 26(16): 2072-2079.

[9] 吕志甲, 贺志勇, 郑强, 等. 载荷和滑动速度对块体镁基非晶合金干摩擦性能的影响[J]. 表面技术, 2018, 47(1): 92-99.
LYU Z J, HE Z Y, ZHENG Q, et al. Effects of Load and Sliding Velocity on Dry Friction Properties of Mg-Based Bulk Metallic Glass[J]. Surface Technology, 2018, 47(1): 92-99.

[10] 王彦芳, 孙旭, 宋增金, 等. 宽带激光熔覆非晶合金涂层界面组织结构[J]. 表面技术, 2018, 47(3): 61-65.
WANG Y F, SUN X, SONG Z J, et al. Interface Microstructures of Broad-Band Laser Cladding Amorphous Alloy Coating[J]. Surface Technology, 2018, 47(3): 61-65.

[11] TIAN L, CHENG Y Q, SHAN Z W, et al. Approaching the Ideal Elastic Limit of Metallic Glasses[J]. Nature Communications, 2012, 3: 609.

[12] INOUE A, TAKEUCHI A. Recent Development and Application Products of Bulk Glassy Alloys[J]. Acta Materialia, 2011, 59(6): 2243-2267.

[13] 司迎迎, 任亚东, 赵永强, 等. 电沉积 Ni-Fe-P 非晶合金析氢阴极材料及其去合金化处理[J]. 表面技术, 2020, 49(9): 175-181.
SI Y Y, REN Y D, ZHAO Y Q, et al. Electrodeposited Ni-Fe-P Amorphous Alloy as Cathode Material for Hydrogen Evolution and Its De-alloying Treatment[J]. Surface Technology, 2020, 49(9): 175-181.

[14] 高鹏飞, 陈永君, 王增睿, 等. 铁基非晶涂层的研究进展与应用[J]. 表面技术, 2023, 52(3): 64-74.
GAO P F, CHEN Y J, WANG Z R, et al. Research Progress and Application of Fe-based Amorphous Coatings[J]. Surface Technology, 2023, 52(3): 64-74.

[15] CHENG Y Q, MA E. Intrinsic Shear Strength of Metallic Glass[J]. Acta Materialia, 2011, 59(4): 1800-1807.

[16] GAO K, ZHU X G, CHEN L, et al. Recent Development in the Application of Bulk Metallic Glasses[J]. Journal of Materials Science & Technology, 2022, 131: 115-121.

[17] LIU Y H, WANG G, WANG R J, et al. Super Plastic Bulk Metallic Glasses at Room Temperature[J]. Science, 2007, 315(5817): 1385-1388.

[18] TAN Y, WANG Y W, CHENG X W, et al. Effects of Al Replacement on Glass Forming Ability and Mechanical Properties of Zr-Based Bulk Metallic Glasses[J]. Journal of Non-Crystalline Solids, 2021, 568: 120962.

[19] LIU Z Q, ZHANG Z F. Strengthening and Toughening Metallic Glasses: The Elastic Perspectives and Opportunities[J]. Journal of Applied Physics, 2014, 115(16): 163505.

[20] HOFMANN D C. Shape Memory Bulk Metallic Glass Composites[J]. Science, 2010, 329(5997): 1294-1295.

[21] WU Y, MA D, LI Q K, et al. Transformation-Induced

Plasticity in Bulk Metallic Glass Composites Evidenced by In-Situ Neutron Diffraction[J]. Acta Materialia, 2017, 124: 478-488.

[22] CHEN Y, TANG C G, JIANG J Z. Bulk Metallic Glass Composites Containing B2 Phase[J]. Progress in Materials Science, 2021, 121: 100799.

[23] ZHANG Y, WANG W H, GREER A L. Making Metallic Glasses Plastic by Control of Residual Stress[J]. Nature Materials, 2006, 5: 857-860.

[24] ZHANG Z F, HE G, ECKERT J, et al. Fracture Mechanisms in Bulk Metallic Glassy Materials[J]. Physical Review Letters, 2003, 91(4): 045505.

[25] ZHAO J X, ZHANG Z F. On the Stress-State Dependent Plasticity of Brittle Metallic Glasses: Experiment, Theory and Simulation[J]. Materials Science and Engineering: A, 2013, 586: 123-132.

[26] QU R T, ZHANG Q S, ZHANG Z F. Achieving Macroscopic Tensile Plasticity of Monolithic Bulk Metallic Glass by Surface Treatment[J]. Scripta Materialia, 2013, 68(11): 845-848.

[27] CHENG Y Y, PANG S J, CHEN C, et al. Size-Dependent Enhancement of Plasticity by Laser Surface Melting in $Zr_{55}Al_{10}Ni_5Cu_{30}$ Bulk Metallic Glass[J]. Journal of Alloys and Compounds, 2016, 658: 49-54.

[28] CHENG Y Y, PANG S J, CHEN C, et al. Tensile Plasticity in Monolithic Bulk Metallic Glass with Sandwiched Structure[J]. Journal of Alloys and Compounds, 2016, 688: 724-728.

[29] CHENG Y Y, PANG S J, CHEN C, et al. Tailoring Residual Stress to Achieve Large Plasticity in $Zr_{55}Al_{10}Ni_5Cu_{30}$ Bulk Metallic Glass[J]. Journal of Alloys and Compounds, 2017, 690: 176-181.

[30] CHEN B Q, LI Y, YI M, et al. Optimization of Mechanical Properties of Bulk Metallic Glasses by Residual Stress Adjustment Using Laser Surface Melting[J]. Scripta Materialia, 2012, 66(12): 1057-1060.

[31] CHEN B Q, PANG S J, HAN P P, et al. Improvement in Mechanical Properties of a Zr-Based Bulk Metallic Glass by Laser Surface Treatment[J]. Journal of Alloys and Compounds, 2010, 504: S45-S47.

[32] ZHAO L, HAN D X, GUAN S, et al. Simultaneous Improvement of Plasticity and Strength of Metallic Glasses by Tailoring Residual Stress: Role of Stress Gradient on Shear Banding[J]. Materials & Design, 2021, 197: 109246.

[33] JIAO Y, BROUSSEAU E, KOSAI K, et al. Softening and Hardening on a Zr-Based Bulk Metallic Glass Induced by Nanosecond Laser Surface Melting[J]. Materials Science and Engineering: A, 2021, 803: 140497.

[34] JANG J S C, JIAN S R, CHANG C F, et al. Thermal and Mechanical Properties of the $Zr_{53}Cu_{30}Ni_9Al_8$ Based Bulk Metallic Glass Microalloyed with Silicon[J]. Journal of Alloys and Compounds, 2009, 478(1/2): 215-219.

[35] LIU C T, CHISHOLM M F, MILLER M K. Oxygen Impurity and Microalloying Effect in a Zr-Based Bulk Metallic Glass Alloy[J]. Intermetallics, 2002, 10(11/12): 1105-1112.

[36] ZHANG J H, LI Y C, WAN F P, et al. The Positive Effect of Non-Inert Casting Atmospheres on the Glass-Forming Ability of FeMoPCBSi Bulk Metallic Glass[J]. Journal of Alloys and Compounds, 2017, 702: 1-5.

[37] CHOI-YIM H, BUSCH R, JOHNSON W L. The Effect of Silicon on the Glass Forming Ability of the $Cu_{47}Ti_{34}Zr_{11}Ni_8$ Bulk Metallic Glass Forming Alloy during Processing of Composites[J]. Journal of Applied Physics, 1998, 83(12): 7993-7997.

[38] JIANG J, WANG Z B, PANG S J, et al. Oxygen Impurity Improving Corrosion Resistance of a Zr-Based Bulk Metallic Glass in 3.5wt.% NaCl Solution[J]. Corrosion Science, 2021, 192: 109867.

[39] LEE J I, KIM S Y, PARK E S. In-Situ Synthesis and Mechanical Properties of Zr-Based Bulk Metallic Glass Matrix Composites Manipulated by Nitrogen Additions[J]. Intermetallics, 2017, 91: 70-77.

[40] LIU C T, LU Z P. Effect of Minor Alloying Additions on Glass Formation in Bulk Metallic Glasses[J]. Intermetallics, 2005, 13(3/4): 415-418.

[41] LU Z P, LIU C T, PORTER W D. Role of Yttrium in Glass Formation of Fe-Based Bulk Metallic Glasses[J]. Applied Physics Letters, 2003, 83(13): 2581.

[42] 黄海博, 孙文磊, 黄勇. 超高速激光熔覆 Fe 基非晶合金单道工艺分析[J]. 表面技术, 2022, 51(7): 410-419.
HUANG H B, SUN W L, HUANG Y. Analysis on the Process of Single Track Fe-based Amorphous Alloy during Ultra High Speed Laser Cladding[J]. Surface Technology, 2022, 51(7): 410-419.

[43] ZHANG L, HUANG H. Micro Machining of Bulk Metallic Glasses: A Review[J]. The International Journal of Advanced Manufacturing Technology, 2019, 100(1): 637-661.

[44] DENG L, GEBERT A, ZHANG L, et al. Mechanical Performance and Corrosion Behaviour of Zr-Based Bulk Metallic Glass Produced by Selective Laser Melting[J]. Materials & Design, 2020, 189: 108532.

[45] PAN J, CHEN Q, LI N, et al. Formation of Centimeter Fe-Based Bulk Metallic Glasses in Low Vacuum Environment[J]. Journal of Alloys and Compounds, 2008, 463(1/2): 246-249.

[46] WANG W H. Roles of Minor Additions in Formation and Properties of Bulk Metallic Glasses[J]. Progress in Materials Science, 2007, 52(4): 540-596.

[47] YANG B J, LU W Y, ZHANG J L, et al. Melt Fluxing to Elevate the Forming Ability of Al-Based Bulk Metallic Glasses[J]. Scientific Reports, 2017, 7: 11053.

[48] ZHENG Q, MA H, MA E, et al. Mg-Cu-(Y, Nd) Pseudo-Ternary Bulk Metallic Glasses: The Effects of Nd on Glass-Forming Ability and Plasticity[J]. Scripta Materialia, 2006, 55(6): 541-544.

（下转第 183 页）

[17] 罗文博. 硬质涂层织构化及其摩擦学试验研究[D]. 秦皇岛: 燕山大学, 2019: 11-19.
LUO W B. Tribological Experiment Study of Textured Hard Coating[D]. Qinhuangdao: Yanshan University, 2019: 11-19.

[18] 李振东, 詹华, 王亦奇, 等. 干摩擦条件下基体粗糙度对 Cr-DLC 薄膜摩擦磨损性能的影响[J]. 摩擦学学报, 2016, 36(6): 741-748.
LI Z D, ZHAN H, WANG Y Q, et al. Effect of Substrate Roughness on Friction and Wear Properties of Cr-DLC Films under Dry-Sliding Condition[J]. Tribology, 2016, 36(6): 741-748.

[19] FERRARI A C, ROBERTSON J. Resonant Raman Spectroscopy of Disordered, Amorphous, and Diamondlike Carbon[J]. Physical Review B, 2001, 64(7): 075414.

[20] ROBERTSON J. Recombination and Photoluminescence Mechanism in Hydrogenated Amorphous Carbon[J]. Physical Review B, Condensed Matter, 1996, 53(24): 16302-16305.

[21] HEITZ T, GODET C, BOURÉE J E, et al. Radiative and Nonradiative Recombination in Polymerlike A–C:H Films[J]. Physical Review B, 1999, 60(8): 6045-6052.

[22] WAGNER A J, WOLFE G M, FAIRBROTHER D H. Reactivity of Vapor-Deposited Metal Atoms with Nitrogen-Containing Polymers and Organic Surfaces Studied by in Situ XPS[J]. Applied Surface Science, 2003, 219(3/4): 317-328.

[23] LI H X, XU T, WANG C B, et al. Annealing Effect on the Structure, Mechanical and Tribological Properties of Hydrogenated Diamond-Like Carbon Films[J]. Thin Solid Films, 2006, 515(4): 2153-2160.

[24] 瞿全炎, 邱万奇, 曾德长, 等. 划痕法综合评定膜基结合力[J]. 真空科学与技术学报, 2009, 29(2): 184-187.
QU Q Y, QIU W Q, ZENG D C, et al. Measurement of TiN Film Substrate Interfacial Adhesion by Scratching[J]. Chinese Journal of Vacuum Science and Technology, 2009, 29(2): 184-187.

[25] LIU Y H, JIANG Y L, SUN J H, et al. Durable Superlubricity of Hydrogenated Diamond-Like Carbon Film Against Different Friction Pairs Depending on Their Interfacial Interaction[J]. Applied Surface Science, 2021, 560: 150023.

[26] HATADA R, FLEGE S, BABA K, et al. Temperature Dependent Properties of Silicon Containing Diamondlike Carbon Films Prepared by Plasma Source Ion Implantation[J]. Journal of Applied Physics, 2010, 107(8): 83307.

（上接第 173 页）

[49] ZHANG Z F, ECKERT J, SCHULTZ L. Difference in Compressive and Tensile Fracture Mechanisms of $Zr_{59}Cu_{20}Al_{10}Ni_8Ti_3$ Bulk Metallic Glass[J]. Acta Materialia, 2003, 51(4): 1167-1179.

[50] SUN B A, TAN J, PAULY S, et al. Stable Fracture of a Malleable Zr-Based Bulk Metallic Glass[J]. Journal of Applied Physics, 2012, 112(10): 103533-103533-6.

[51] CHEN S S, ZHANG H R, TODD I. Phase-Separation-Enhanced Plasticity in a $Cu_{47.2}Zr_{46.5}Al_{5.5}Nb_{0.8}$ Bulk Metallic Glass[J]. Scripta Materialia, 2014, 72/73: 47-50.

[52] CHEN S H, DING D, YU P, et al. Hierarchical Amorphous Structures in a $Zr_{50}Cu_{42}Al_8$ Bulk Metallic Glass[J]. Materials Science and Engineering: A, 2015, 639: 75-79.

[53] QU R T, ZHANG Z F. A Universal Fracture Criterion for High-Strength Materials[J]. Scientific Reports, 2013, 3: 1117.

[54] YUAN C C, XIANG J F, XI X K, et al. NMR Signature of Evolution of Ductile-to-Brittle Transition in Bulk Metallic Glasses[J]. Physical Review Letters, 2011, 107(23): 236403.

[55] ZHENG N, QU R T, PAULY S, et al. Design of Ductile Bulk Metallic Glasses by Adding "Soft" Atoms[J]. Applied Physics Letters, 2012, 100(14): 141901.

[56] CONNER R D, MAIRE R E, JOHNSON W L. Effect of Oxygen Concentration Upon the Ductility of Amorphous $Zr_{57}Nb_5Al_{10}Cu_{15.4}Ni_{12.6}$[J]. Materials Science and Engineering: A, 2006, 419(1/2): 148-152.

[57] HAN Z H, HE L, HOU Y L, et al. Understanding the Mechanism for the Embrittlement of a Monolithic Zr-Based Bulk Metallic Glass by Oxygen[J]. Intermetallics, 2009, 17(7): 553-561.

[58] LU Z P, BEI H, WU Y, et al. Oxygen Effects on Plastic Deformation of a Zr-Based Bulk Metallic Glass[J]. Applied Physics Letters, 2008, 92(1): 011915.

[59] NAKAI Y, FUJIHARA K, SEI N, et al. Fatigue Crack Initiation and Propagation at a Sharp Notch in Zr-Based Bulk Metallic Glass[J]. Materials Science Forum, 2010, 638/639/640/641/642: 1659-1664.